DOI: 10.1002/cphc.200900941

Photovoltaic Universal Joints: Ball-and-Socket Interfaces in Molecular Photovoltaic Cells

Noah J. Tremblay,[a] Alon A. Gorodetsky,[a] Marshall P. Cox,[b] Theanne Schiros,[c] Bumjung Kim,[a] Rachel Steiner,[d] Zachary Bullard,[d] Aaron Sattler,[a] Woo-Young So,[e] Yoshimitsu Itoh,[a] Michael F. Toney,[f] Hirohito Ogasawara,[f] Arthur P. Ramirez,[g] Ioannis Kymissis,*[b] Michael L. Steigerwald,[a] and Colin Nuckolls*[a]

Herein, we detail how to grow one crystalline organic semiconductor on another epitaxially and thereby provide a method to tune the electronic nature of the *p*–*n* junction in organic photovoltaics (OPVs). While OPVs are attractive as materials for conversion of sunlight into electrical energy,[1] higher conversion efficiencies[2] are needed for OPVs to become a viable technology.[3–6] Regardless of the type of OPV, either a bilayer[7] or bulk-heterojunction (BHJ)[4] (Figure 1 A), the interface between the hole and electron transporting films is the critical locus for exciton formation and dissociation.[8–11] In inorganic materials, the interface between two semiconductors is crucially important in determining and controlling the electrical properties of these materials and is controlled by a heteroepitaxial growth of one crystalline material on another. We show here that *p*-type and *n*-type organic semiconductors can be designed to have nested shapes that create an epitaxial growth that achieves higher conversion efficiencies and open circuit voltages in these devices to within 10% of the theoretical limit. We utilize the class of molecules known as contorted hexabenzocoronenes (HBCs, Figure 1 B) because they are established *p*-type semiconductors[12–14] and are also photoconductive.[15,16] This HBC has an unusual shape in that it is contorted and doubly-concave.[12] The size and shape of this molecule are complementary to buckminsterfullerene (C_{60}), which is a well-known *n*-type semiconductor (Figure 1 C). It is this potential for shape and electronic complementarity between these two molecular structures that led us to investigate them in the context of heteroepitaxial growth.

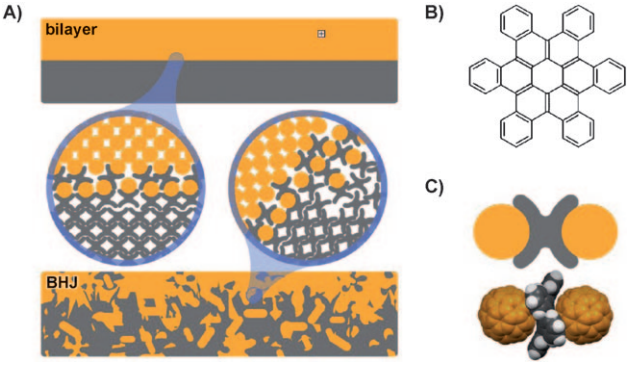

Figure 1. A) Depiction of ball-and-socket interfaces in bilayer and bulk heterojunction devices. B) Chemical structure of the *contorted*-HBC. C) Correlation between depiction (top) and molecular structure from the co-crystal of HBC and C_{60} (bottom).

We first focused on whether HBC and C_{60} formed co-crystalline, supramolecular assemblies. Two experiments, one from solution (Figure 2 A) and one from the gas phase (Figure 2 B) show that the materials form co-crystals. Large purple-gray crystals were produced from a saturated solution of C_{60} and HBC in chlorobenzene.

The molecular structure determined from the solution-grown crystals reveals that HBC and C_{60} spontaneously formed an interdigitated supramolecular complex (complex **1**). The three-dimensional structure of HBC comprises two opposing concave aromatic faces, wherein a C_{60} had nestled into each face (Figure 2 A). It is important to note that a number of organic molecules have been specifically designed to form complementary interactions with C_{60} and have yielded co-crystals.[17–20] However, few of these molecules are suitable candidates for the formation of a *p*–*n* junction.[17]

The crystal of **1** comprises C_{60}, HBC, and chlorobenzene (2:1:1), wherein HBC and C_{60} organize into a repeating pattern of ABAABA as shown in Figure 2 A. Each HBC has two C_{60} nearest neighbors, and each C_{60} has one HBC nearest neighbor and one C_{60} nearest neighbor. The C_{60} is centered over one of the

[a] *N. J. Tremblay, Dr. A. A. Gorodetsky, B. Kim, A. Sattler, Dr. Y. Itoh, Dr. M. L. Steigerwald, Prof. C. Nuckolls*
Department of Chemistry and
The Center for Electron Transport in Molecular Nanostructures
Columbia University, New York, NY 10027 (USA)
Fax: (+1) 212-932-1289
E-mail: cn37@columbia.edu

[b] *M. P. Cox, Dr. I. Kymissis*
Department of Electrical Engineering
Columbia University, New York, NY 10027 (USA)
Fax: (+1) 212-932-9421
E-mail: johnkym@ee.columbia.edu

[c] *Dr. T. Schiros*
The Center for Electron Transport in Molecular Nanostructures
Current Affiliation: Columbia Energy Frontier Research Center (EFRC)
Columbia University, New York, NY 10027 (USA)

[d] *R. Steiner, Z. Bullard*
Department of Materials Science and Engineering
The Center for Electron Transport in Molecular Nanostructures
Columbia University, New York, NY 10027 (USA)

[e] *Dr. W.-Y. So*
Department of Applied Physics and Applied Mathematics
Columbia University, New York, NY 10027 (USA)

[f] *Dr. M. F. Toney, Dr. H. Ogasawara*
Stanford Synchrotron Radiation Lightsource
Menlo Park, CA 94035 (USA)

[g] *Prof. A. P. Ramirez*
The Jack Baskin School of Engineering
University of California - Santa Cruz
Santa Cruz, CA 95064 (USA)

Supporting information for this article is available on the WWW under http://dx.doi.org/10.1002/cphc.200900941.

 © 2010 Wiley-VCH Verlag GmbH & Co. KGaA, Weinheim

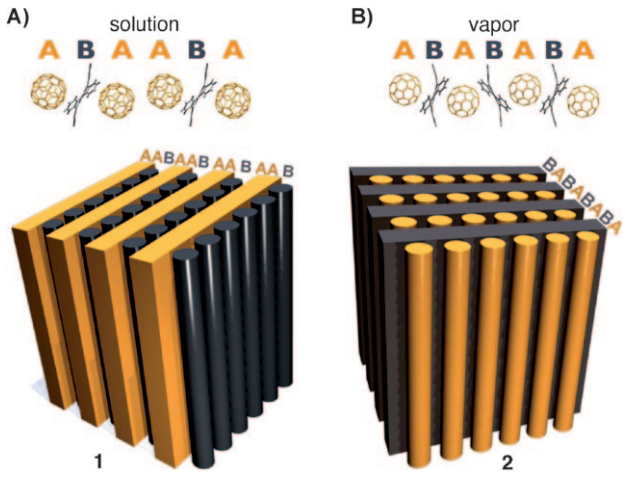

Figure 2. Organization of HBC and C_{60} in co-crystals of C60 and HBC A) from solution as complex **1** and B) from the gas phase as complex **2**.

six-membered rings on the edge of the coronene core of HBC; in this instance, the vertical π–π distance is 3.00 Å.

We were also able to co-crystallize these molecules without solvent using horizontal physical vapor transport.[21] We placed HBC and C_{60} powders in the hot zone (550 °C) of a horizontal, gradient-temperature furnace. Crystals (complex **2**) formed in the cold zone of the furnace (330 °C). The composition of **2** was 1:1 HBC:C_{60} (Figure 2B).

The assembly of HBC and C_{60} in **2** is different from **1**. The HBC and C_{60} organize in an ABAB repeating pattern in **2** (Figure 2B). In this structure there are two crystallographically inequivalent HBC sites. Every HBC has two C_{60} nearest neighbors with the C_{60} having two non-identical HBC neighbors. Each C_{60} is centered directly in the middle of the core six-membered ring in one type of HBC at a π–π distance of 2.93 Å. Each C_{60} is also centered over another HBC just outside one of the bonds of the core six-membered ring at a π–π distance of 3.07 Å. The HBC molecules in **2** are organized in sheets (Figure 2B). Even though there are two inequivalent HBC sites, they are assembled into a rectangular array with a center-to-center distance of 11.36 Å. Every HBC molecule has a 3.63 Å close carbon-to-carbon contact with four neighboring HBCs.

The C_{60} molecules in **2** form columns (Figure 2B). The center-to-center distance between the columns is 9.88 Å, which is one of the shortest C_{60}–C_{60} distances reported to date.[22,23] The fullerenes assemble in a zigzag pattern with a 111° bend (center-to-center) at each C_{60}. The columns are spaced 15.87 Å apart from one another. A spacing of 9.88 Å is within the range of previously reported values for C_{60}–C_{60} spacings in the pure crystal, but 15.87 Å is significantly larger than those values, indicating that C_{60} forms columns in **2**.

The solution-grown crystals of **1** were large enough that we were able to directly measure the resistance of single crystals using evaporated silver electrodes (Figure 3). These crystals are insulating, which is expected as both HBC and C_{60} individually are semiconductors. The resistance was significantly reduced after the same species was kept in vacuum at room temperature for twelve days. We presume that this is due to the slow evaporation of chlorobenzene. Illumination of the devices causes a 1,000-fold decrease in resistance. Crystals of **2** were not large enough to measure in single-crystal devices.

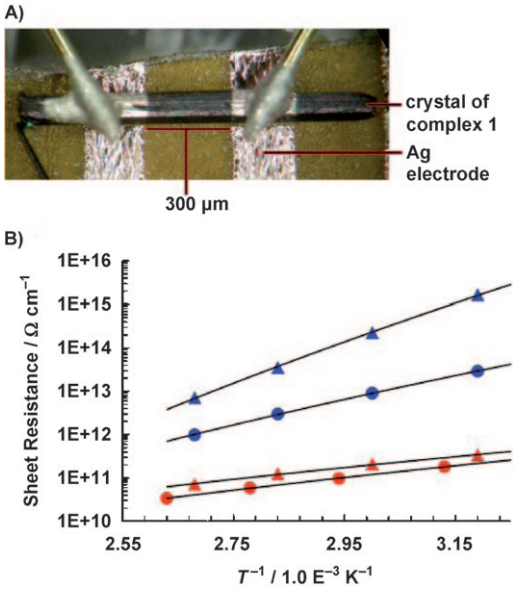

Figure 3. A) Single-crystal device of complex **1**. B) Inverse temperature vs sheet resistance of the device measured before annealing (triangles), after annealing (circles), with illumination (red), and without illumination (blue).

We made OPV devices to test our hypothesis that the large decrease in resistance in the crystals is due to charge transfer between the *n*- and *p*-type molecules. We chose an OPV bilayer architecture (Figure 4A) rather than a BHJ architecture because it is easier to optimize the former. We used an electrode pattern that allowed for rapid and reproducible electronic characterization of over 200 devices at a time. Standard electrode materials were deliberately used for all devices for direct comparison to literature values.[24] We measured the electrical characteristics of these devices in the dark, and then again when they were exposed to a 1.5 AM solar-simulated light source (power density = 1 sun, 100 mW cm^2). The devices were open to air during the measurements unless otherwise noted.

The illumination-dependent current density/voltage characteristics of an HBC/C_{60} device appear in Figure 4B: a short-circuit current density (J_{SC}) of 3.32 mA/cm^2, open-circuit voltage (V_{OC}) of 0.88 V, and a fill factor of 0.27 yield an efficiency of 0.77%. These values are not high enough to be viable in technology, but are very good given the poor absorbance of the HBC and the high V_{OC} in the device. It charts a path to more efficient devices that would shift the absorbance of the HBC to absorb more broadly in the solar region of the spectrum As support for this, the normalized external quantum efficiency (EQE) spectra show the highest value for the relative efficiency near 390 nm. This is close to the maximum in the absorbance of the HBC thin film (Figures S1 and S2, Supporting Information).

The efficiency of a photovoltaic device is proportional to the magnitude of the V_{OC}. To a first approximation, the theoretical

 © 2010 Wiley-VCH Verlag GmbH & Co. KGaA, Weinheim

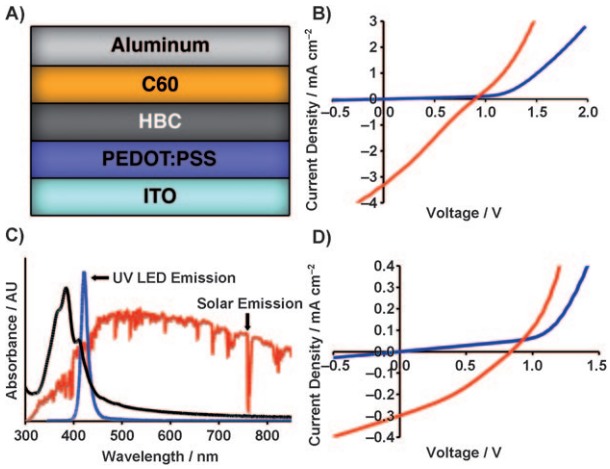

Figure 4. A) OPV device architecture: PEDOT:PSS (25 nm), HBC (25 nm), C_{60} (40 nm), aluminum (60 nm). Device are is 0.16 cm^2. B) *J–V* characteristics of *contorted*-HBC OPVs in the dark (blue) and illuminated with 1.5 AM solar simulated light source (red). C) Absorbance spectrum of a thin film of *contorted*-HBC (black) overlaid with the emission of the UV LED light source (blue) and the solar spectrum (red). D) *J–V* characteristics of *contorted*-HBC OPVs in the dark (blue) and illuminated with UV LED light source at 422 nm and an intensity of 1.5 mW cm^2 (red).

maximum V_{OC} for our devices is the energy difference between the highest occupied molecular orbital (HOMO) of HBC at ~5.5 eV and the lowest unoccupied molecular orbital (LUMO) of C_{60} at ~4.5 eV. Our V_{OC}s approach this difference of 1.0 V. These are among the highest values reported for OPVs.[3]

The efficiency of a photovoltaic device is also directly proportional to the J_{SC}. Upon illumination, the current density of the HBC/C_{60} devices clearly increases, regardless of the applied bias. This is consistent with our observations of photoconductivity[15,16] in HBC films and HBC/C_{60} co-crystals (Figure 3).

The device performance observed here is unexpectedly good given that the absorbance of HBC overlaps poorly with the simulated solar spectrum (Figure 4C). When the devices were irradiated at 422 nm near the maximum of the normalized EQE spectrum, we observed conversion efficiencies of up to 5.7% (Figure 4D).[25] There is only a slight change in the average V_{OC} of these devices upon moving from solar to UV LED illumination (Figure 4B, 4D). The performance of HBC/C_{70} devices is essentially the same as that of HBC/C_{60} devices (Figure S3, Supporting Information). All the devices were operated in ambient atmosphere without any encapsulation.

We have seen that HBC and C_{60} form a tight molecular complex. We have also seen that bilayer OPV devices using these two compounds have good functional performance. We have previously used grazing incidence X-ray diffraction (GIXD) to detect co-crystalline regions within polymer/fullerene BHJs[26] and herein we use the same technique to analyze the HBC/C_{60} interface. We collected GIXD data from HBC-coated silicon substrates after stepwise depositions of C_{60} onto the HBC (25 nm). We increased the thickness (*x* nm) of the C_{60} layer from 0 nm to the optimal device thickness of 40 nm (Figure 5).

The film of pure HBC shows weak crystalline order; a weak (100) reflection at $Q = \sim 0.5$ Å^{-1}, labeled "A" in Figure 5, is largely confined to the vertical direction (Q_z) and indicates that the HBC molecules are oriented within a 5–10° tilt from the surface normal, while the breadth of the peak indicates small crystallite

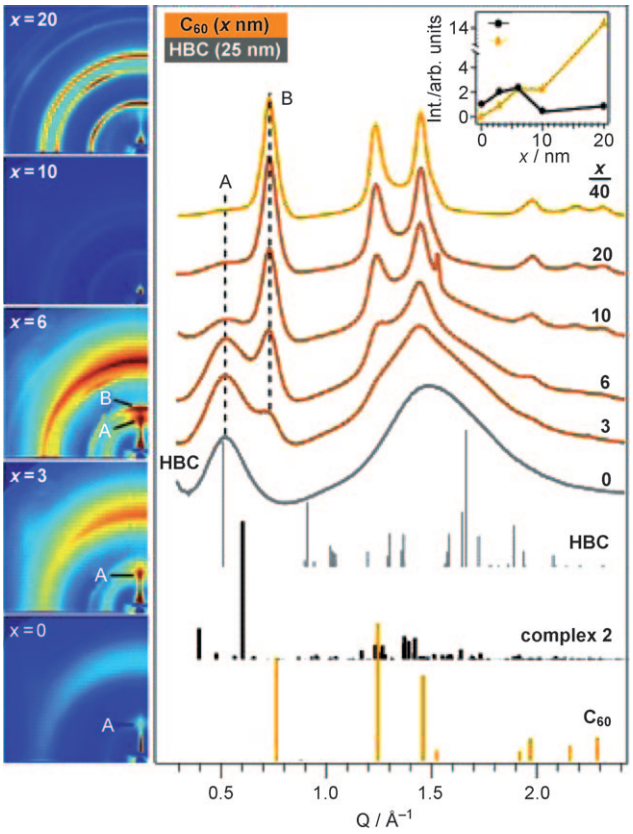

Figure 5. GIXD measurements (2D images on the left and integrated intensity on the right) for films of C_{60} (40 nm), bilayers of increasing thickness of C_{60} on HBC, and pure HBC (25 nm). HBC, complex 2 and C_{60} reflections obtained from powder samples are also shown. Integrated intensities of the diffraction pattern are normalized by the maximum peak height; 2D images for $x = 0$–10 nm share the same intensity scale while $x \geq 20$ nm has a larger upper limit due to the thickness of the film (see inset for peak intensity). Peak A corresponds to diffraction intensity which increases in intensity at the HBC/C_{60} interface before disappearing under the C_{60} signal. Note: the sharp peak appearing at $Q = 1.53$ Å^{-1} in the 10 nm C_{60} data corresponds to the (222) reflection of pure C_{60}.

domains. The broad peak centered at $Q = \sim 1.5$ Å^{-1} is dominated by the signal from the SiO_2 substrate which overwhelms that of any HBC reflections. When 3–6 nm of C_{60} is deposited on top of the HBC film, the intensity of peak A increases significantly along the vertical, and C_{60} peaks [$Q = \sim 0.75$ (peak B), 1.24 and 1.5 Å^{-1}] also appear. However, in the absence of an interaction between HBC and C_{60}, the (100) reflection from pure HBC should be damped rather than enhanced by a thin C_{60} layer at grazing incidence. Instead, we find that while the intensity of the C_{60} peaks increase linearly with increasing film thickness for all deposition steps, the intensity of peak A *increases* for thin C_{60} films ($x \leq 6$ nm), that is, at the interfacial region, before decreasing as it becomes buried by the C_{60} (see Figure 5 inset). The increase in intensity of peak A suggests the C_{60} introduces an additional degree of order at the bilayer in-

 © 2010 Wiley-VCH Verlag GmbH & Co. KGaA, Weinheim

terface. Since reflections due to complex **2** appear in the *Q*-region of A while C_{60} reflections do not (Figure 5), we anticipate that, under the present conditions, deposition of C_{60} on the HBC surface would result in the formation of some small co-crystalline regions at the interface. This interpretation is supported by the shift of the (111) reflection of C_{60} (peak B) from its nominal position (0.73 $Å^{-1}$) to lower Q (0.7 $Å^{-1}$), toward the co-crystal reflections, for the 3 nm C_{60} film, as well as the width of peak A, which is roughly consistent with a 3 nm interface layer.

To further probe the local electronic and geometric structure of the HBC/C_{60} interface, it was investigated with surface-sensitive X-ray photoelectron (XPS) and near-edge X-ray absorption spectroscopy (NEXAFS). For this experiment, the interface was modeled by depositing 2 nm C_{60} on a 10 nm HBC film on ITO. The spectral differences between the C_{60} (2 nm)/HBC(10 nm) bilayer and pristine (10 nm) films of either HBC or C_{60} then afforded insight into the unique interaction between the shape complementary donor and acceptor molecules.

XPS probing the C 1s region (Figure S4, Supporting Information) provides direct evidence for an electronic interaction between C_{60} and HBC in the deposited films. Specifically, relative to the pure HBC and C_{60} films, the bilayers have a shift to higher binding energy by 0.2 eV, a change in peak shape, and a narrowing in peak width. Such features are consistent with charge transfer at donor-acceptor interface, which affects the ability of the system to screen and stabilize the core-ionized final state, thereby altering the shape, width[27] and energy[28–29] of the photoemission peak. This supports the presence of an intimate interaction between the donor and acceptor molecules.

Surface-sensitive, polarization-dependent NEXAFS, shown in Figure S4 (Supporting Information), indicates that the electronic interaction between acceptor and donor is accompanied by a physical ordering of the molecules at the HBC/C_{60} interface. In the total electron yield (TEY) signal, which probes the bulk of the 10 nm films, no polarization dependence is observed, indicating the lack of a preferred molecular orientation in the film. However, an anisotropy in bond geometry is uniquely observed for the HBC/C_{60} bilayer in the Auger electron yield (AEY) signal, which probes the ~1–2 nm near-surface region; that is, the HBC/C_{60} interface. From the polarization dependence of the integrated π^* resonances,[28–31] we estimate that the HBC molecules interacting with C_{60} are oriented at an average tilt angle of ~40° with respect to the surface plane. If the HBC ordering is related to a spontaneous assembly of the molecular partners at the bilayer interface into complex **2**, this HBC tilt angle orients the (110) plane of the co-crystal parallel to the surface plane. In this geometry, X-rays diffracted from the (110) plane of complex **2** would contribute intensity confined to the Q_z direction at $Q = 0.48$ $Å^{-1}$ and thereby explain the increase in peak A in the GIXD data at the HBC/C_{60} interface (Figure 5). The data suggests that there is sufficient solid-state and surface mobility of the molecular partners for coalescence into an ordered state at the interface that can be modeled by the "ball and socket" structure shown in Figure 2.

The sequential deposition of the two shape-complementary molecules thus does produce an interface that is at least partially organized. Do the OPVs benefit from this molecular organization? To assess this we tested *p*-type molecules that lack the doubly-concave distortion from planarity of our HBC but is otherwise very similar. Flat hexa-peri-hexabenzocoronene (*flat*-HBC) is an excellent candidate for comparison to the HBC under investigation (*contorted*-HBC) (Figure S5, Supporting Information). These two molecules have similar electronic structures, band gaps, molecular weights, chemical formulas, evaporation temperatures, molecular dimensions, and UV/Vis absorption spectra in thin films (Figure S2, Supporting Information). The most obvious difference between *flat*-HBC and our *contorted*-HBC is shape: one is perfectly flat while the other is severely distorted from planarity. While the *contorted*-HBC is shape-complementary to fullerenes, the *flat*-HBC is not.

Devices made with the two HBC molecules behaved quite differently under simulated solar irradiation. Devices based on *contorted*-HBC are more efficient than those based on *flat*-HBC (0.55% versus 0.07%). The former also have higher V_{OC}s than the latter (0.84 V versus 0.19 V, Figure S3, Supporting Information). This supports the notion that shape complementarity contributes to the higher V_{OC} values for *contorted*-HBC.

Notably, under UV-LED irradiation, *contorted*-HBC device outperformed *flat*-HBC by more than two orders of magnitude (average efficiencies of $\eta = 3.36\%$ versus 0.03%, Figure S6, Supporting Information). The emission spectrum of the UV-LED covers the longest-wavelength absorbance shoulder for thin films of both HBCs (Figures 2C and S2, Supporting Information). Although *contorted*-HBC devices had V_{OC}s similar to those of *flat*-HBC devices under solar irradiation, the V_{OC}s of *contorted*-HBC devices were over ten times greater than *flat*-HBC (0.80 V versus 0.07 V) under UV light. These results further support our assertion that the shape-complementary interface is essential for peak device performance.

In summary, we reported that shape complementarity improves the donor/acceptor interface and, consequently, the photovoltaic properties of bilayer OPVs. We showed that *contorted*-HBC forms intimate complexes with the fullerenes. We also showed that differences in complementarity directly translate to differences in OPV performance. Better shape complementary improves the interface between donor and acceptor materials in our devices and leads to some of the highest V_{OC}s reported to date, with a maximum of 0.95 V. We also observe efficiencies of up to 5.7% in ambient atmosphere for narrow-width UV irradiation and 1.04% for solar illumination. This data indicates that our OPV cells may be ideally partnered with longer wavelength absorbing layers to achieve higher efficiency solar cells.

Acknowledgements

We acknowledge financial support in part from the Nanoscale Science and Engineering Initiative of the National Science Foundation under NSF Award Number CHE-0641523, in part from the Center for Re-Defining Photovoltaic Efficiency Through Molecule

 © 2010 Wiley-VCH Verlag GmbH & Co. KGaA, Weinheim

Scale Control, an Energy Frontier Research Center funded by the U.S. Department of Energy, Office of Science, Office of Basic Energy Sciences under Award Number DE-SC0001085, and in part from the Chemical Sciences, Geosciences and Biosciences Division, Office of Basic Energy Sciences, US D.O.E. (#DE-FG02-01ER15264) and US D.O.E. (#DE-FG02-04ER46118). We thank Prof. Gerard Parkin for assistance in solving the crystal structure. The National Science Foundation (CHE-0619638) is thanked for acquisition of the X-ray diffractometer and for CHE-0717518. Portions of this research were carried out at the Stanford Synchrotron Radiation Lightsource, a national user facility operated by Stanford University on behalf of the U.S. Department of Energy, Office of Basic Energy Sciences.

Keywords: conducting materials · crystal growth · energy conversion · interfaces · nanotechnology

[1] M. T. Lloyd, J. E. Anthony, G. G. Malliaras, *Materials Today* **2007**, *10*, 34 – 41.
[2] G. Dennler, M. C. Scharber, T. Ameri, P. Denk, K. Forberich, C. Waldauf, C. J. Brabec, *Adv. Mater.* **2008**, *20*, 579 – 583.
[3] B. C. Thompson, J. M. J. Fréchet, *Angew. Chem.* **2008**, *120*, 62 – 82; *Angew. Chem. Int. Ed.* **2008**, *47*, 58 – 77.
[4] G. Yu, J. Gao, J. C. Hummelen, F. Wudl, A. J. Heeger, *Science* **1995**, *270*, 1789 – 1791.
[5] J. Y. Kim, K. Lee, N. E. Coates, D. Moses, T. Q. Nguyen, *Science* **2007**, *317*, 222 – 225.
[6] S. Wenger, S. Seyrling, A. N. Tiwari, M. Grätzel, *Appl. Phys. Lett.* **2009**, *94*, 173508/1 – 173508/3.
[7] C. Tang, *Appl. Phys. Lett.* **1986**, *48*, 183 – 185.
[8] R. D. Kennedy, A. L. Ayzner, D. D. Wanger, C. T. Day, M. Halim, S. I. Khan, S. H. Tolbert, B. J. Schwartz, Y. Rubin, *J. Am. Chem. Soc.* **2008**, *130*, 17290 – 17292.
[9] J. van Herrikhuyzen, A. Syamakumari, A. Schenning, E. Meijer, *J. Am. Chem. Soc.* **2004**, *126*, 10021 – 10027.
[10] X. Yang, J. Loos, *Macromolecules* **2007**, *40*, 1353 – 1362.
[11] B. Schmaltz, T. Weil, K. Mullen, *Adv. Mater.* **2009**, *21*, 1067 – 1078.
[12] S. Xiao, Q. Miao, S. Sanaur, K. Pang, M. L. Steigerwald, C. Nuckolls, *Angew. Chem.* **2005**, *117*, 7556 – 7560; *Angew. Chem. Int. Ed.* **2005**, *44*, 7390 – 7394.
[13] S. Xiao, J. Tang, T. Beetz, X. Guo, N. Tremblay, T. Siegrist, Y. Zhu, M. L. Steigerwald, C. Nuckolls, *J. Am. Chem. Soc.* **2006**, *128*, 10700 – 10702.
[14] X. Guo, M. Myers, S. Xiao, M. Lefenfeld, R. Steiner, G. S. Tulevski, J. Tang, J. Baumert, F. Leibfarth, J. T. Yardley, M. L. Steigerwald, P. Kim, C. Nuckolls, *Proc. Natl. Acad. Sci. USA* **2006**, *103*, 11452 – 11456.
[15] X. Guo, S. Xiao, M. Myers, Q. Miao, M. L. Steigerwald, C. Nuckolls, *Proc. Natl. Acad. Sci. USA* **2009**, *106*, 691 – 696.
[16] Y. Cohen, S. Xiao, M. L. Steigerwald, C. Nuckolls, C. Kagan, *Nano Lett.* **2006**, *6*, 2838 – 2841.
[17] Z. Wang, F. Dötz, V. Enkelmann, K. Müllen, *Angew. Chem. Int. Ed. Angew. Chem. Int. Ed.* **2005**, *44*, 1247 – 1250.
[18] D. Pham, J. Ceron-Bertran, M. M. Olmstead, M. Mascal, A. L. Balch, *Cryst. Growth Des.* **2007**, *7*, 75 – 82.
[19] D. V. Konarev, S. S. Khasanov, A. Otsuka, G. Saito, R. N. Lyubovskaya, *J. Am. Chem. Soc.* **2006**, *128*, 9292 – 9293.
[20] J. L. Atwood, L. J. Barbour, M. W. Heaven, C. L. Raston, *Angew. Chem.* **2003**, *115*, 3376 – 3379; *Angew. Chem. Int. Ed.* **2003**, *42*, 3254 – 3257.
[21] R. A. Laudise, C. Kloc, P. G. Simpkins, T. Siegrist, *J. Cryst. Growth* **1998**, *187*, 449 – 454.
[22] D. L. Dorset, M. P. McCourt, *Acta Crystallogr. A* **1994**, *50*, 344 – 351.
[23] W. I. F. David, R. M. Ibberson, J. C. Matthewman, K. Prassides, T. J. S. Dennis, J. P. Hare, H. W. Krote, R. Taylor, D. R. M. Walton, *Nature* **1991**, *353*, 147 – 149.
[24] J. Peet, M. Senatore, A. J. Heeger, G. Bazan, *Adv. Mater.* **2009**, *21*, 1521 – 1527.
[25] Average UV LED data: efficiency = 3.4 %; J_{sc} = 0.16 mA cm^2; V_{oc} = 0.80 V; FF = 0.23.
[26] A. C. Mayer, M. F. Toney, S. R. Scully, J. Rivnay, C. J. Brabec, M. Scharber, M. Koppe, M. Heeney, I. McCulloch, M. D. McGehee, *Adv. Funct. Mater.* **2009**, *19*, 1173 – 1179.
[27] A. Nilsson, H. Tillborg, N. Martensson, *Phys. Rev. Lett.* **1991**, *67*, 1015 – 1018.
[28] G. Polzonetti, C. Battocchio, A. Goldoni, R. Larciprete, V. Carravetta, R. Paolesse, M. V. Russo, *Chem. Phys.* **2004**, *297*, 307 – 314.
[29] P. Vilmercati, C. Castellarin Cudia, R. Larciprete, C. Cepek, G. Zampieri, L. Sangaletti, S. Pagliara, A. Verdini, A. Cossaro, L. Floreano, A. Morgante, L. Petaccia, S. Lizzit, C. Battocchio, G. Polzonetti, A. Goldoni, *Surf. Sci.* **2006**, *600*, 4018 – 4022.
[30] J. Stöhr, in *NEXAFS Spectroscopy.* Springer-Verlag, Berlin, **1982**, p. 275 – 291.
[31] D. M. DeLongchamp, E. K. Lin, D. Fischer, in *Organic Field-Effect Transistors IV*, edited by Z. Bao and D. J. Gundlach, *Proc. of SPIE* **2005** Vol. 5940, 59400 A1 – 5.

Received: December 1, 2009
Published online on February 15, 2010

 © 2010 Wiley-VCH Verlag GmbH & Co. KGaA, Weinheim